Journal of Alloys and Compounds 723 (2017) 580–588

Contents lists available at ScienceDirect

Journal of Alloys and Compounds

journal homepage: http://www.elsevier.com/locate/jalcom

# Crystal structure, Raman spectroscopy and microwave dielectric properties of $Ba_{3.75}Nd_{9.5}Ti_{18-z}(Al_{1/2}Nb_{1/2})_zO_{54}$ ceramics

Zhe Xiong [a, b], Bin Tang [a, b, *], Zixuan Fang [a, b], Chengtao Yang [a, b], Shuren Zhang [a, b]

[a] National Engineering Research Center of Electromagnetic Radiation Control Materials, University of Electronic Science and Technology of China, Jianshe Road, Chengdu, 610054, People's Republic of China
[b] State Key Laboratory of Electronic Thin Films and Integrated Devices, University of Electronic Science and Technology of China, Jianshe Road, Chengdu, 610054, People's Republic of China

ARTICLE INFO

*Article history:*
Received 2 April 2017
Received in revised form
11 June 2017
Accepted 23 June 2017
Available online 24 June 2017

*Keywords:*
Microwave ceramics
Substitution
Rietveld analysis
Raman spectroscopy

ABSTRACT

The influences of substitution of $(Al_{1/2}Nb_{1/2})^{4+}$ on the crystal structure, Raman spectroscopy and microwave dielectric properties in $Ba_{3.75}Nd_{9.5}Ti_{18}O_{54}$ (BNT) ceramics were investigated in this work. The sintering samples were mainly measured by SEM, XRD and Raman spectrometer. The results showed that all $Ba_{3.75}Nd_{9.5}Ti_{18-z}(Al_{1/2}Nb_{1/2})_zO_{54}$ (BNT-(AN)$z$) samples formed the orthorhombic tungsten-bronze type like structure. Lattice parameters of BNT-(AN)$z$ samples were refined by Rietveld method, and unit cell volume of samples decreased as $z$ increased. The blue shift of Raman spectral peaks was confirmed to the result of Rietveld refinement. Moreover, Raman spectra revealed that flexible oxygen octahedra networks became stressed-rigid and oxygen octahedra became more tilted, which was ascribed to $Al^{3+}$ and $Nb^{5+}$ occupational disorder when $(Al_{1/2}Nb_{1/2})^{4+}$ substituted for $Ti^{4+}$. With increase of $z$ value, the dielectric constant ($\varepsilon_r$) and temperature coefficient of resonant frequency ($\tau_f$) decreased. The BNT-(AN)2 ceramic sintered at 1375 °C for 4 h exhibited excellent microwave dielectric properties: $\varepsilon_r$ = 73.9, $Q\times f$ = 13,177 GHz, and $\tau_f$ = +0.3 ppm/°C. The relationship of the bond valence of the B-site to Raman shift of the $A_g$ mode, dielectric constant ($\varepsilon_r$) and $\tau_f$ were analyzed.



## 1. Introduction

In recent years, the rapid progress of modern wireless communication applications, such as wireless charging, Virtual Reality (VR) and self-driving technology has stimulated the development of microwave dielectric ceramics to meet the demand of microwave device including resonators, oscillator and wave guides [1,2]. With respect to microwave applications, the materials should have high relative permittivity ($\varepsilon_r$), high quality factor ($Q\times f$) and near zero temperature coefficient of resonant frequency ($\tau_f$), which are necessary to achieve high miniaturization, integration and reliability in microwave communication system [3].

For decades, $Ba_{6-3x}Nd_{8+2x}Ti_{18}O_{54}$ solid solution-based ceramics have drawn an increasing interest for their high $\varepsilon_r$ and high $Q\times f$ value, and they have attracted many scientific research personnel to study them. In 1996, Negas [4] studied the microwave dielectric properties of $Ba_{6-3x}Nd_{8+2x}Ti_{18}O_{54}$ ceramics as $x$ value changes. What's more, many senior scientists have investigated the structure of $BaO\text{-}Nd_2O_3\text{-}TiO_2$ ternary compounds by various analysis methods, and they all announced that the crystal structure of $Ba_{6-3x}Nd_{8+2x}Ti_{18}O_{54}$ ceramics contained elements of tungsten–bronze [5–8]. As shown in Fig. 1, the 2 × 2 perovskite block took shape in tungsten-bronze type like structure, $Ti^{4+}$ and $O^{2-}$ formed titanium-oxygen octahedra [$TiO_6$], then $Ba^{2+}$ and $Nd^{2+}$ occupied A1, A2 site respectively in titanium-oxygen octahedra [$TiO_6$] interstice. It was reported that the $\tau_f$ value of $Ba_{6-3x}Nd_{8+2x}Ti_{18}O_{54}$ solid solution series were affected by tilting of the $TiO_6$ octahedra [9–11]. But their large positive $\tau_f$ value (+65 to +130 ppm/°C) always retarded their wide utilization [8,12,13]. Among $Ba_{6-3x}Nd_{8+2x}Ti_{18}O_{54}$ solid solutions series, the excellent properties of $Ba_{3.75}Nd_{9.5}Ti_{18}O_{54}$($x$ = 3/4) (BNT) ceramics ($\varepsilon_r \geq 80$, $Q\times f \geq 9000$ GHz, $\tau_f$ ~70 ppm/°C) deserves further attention [13,14]. Many researchers have studied modified $Ba_{6-3x}Nd_{8+2x}Ti_{18}O_{54}$ solid solutions. For example, Nenasheva et al. determined the $Zr^{4+}$substitution was in favour of lower $\tau_f$ in $BaNd_2Ti_4O_{12}$ ceramics but resulted in deteriorative $\varepsilon_r$ and $Q\times f$ values [15]. Later, the $Ba_4(Sm_{0.5}Nd_{0.5})_{28/3}Ti_{18}O_{54}$ and $Ba_4Nd_{9.33}$-

* Corresponding author. State Key Laboratory of Electronic Thin Films and Integrated Devices, University of Electronic Science and Technology of China, Jianshe Road, Chengdu, 610054, People's Republic of China.
*E-mail address:* tangbin.uestc@gmail.com (B. Tang).

http://dx.doi.org/10.1016/j.jallcom.2017.06.258
0925-8388/

$Ti_{18}O_{54}$ with $Al_2O_3$ addition were synthesized by Chang [16] and Yao [17] respectively. Huang et al. [18]. Reported that $(Ba_{1-x}Sr_x)4(Sm_{0.4}Nd_{0.6})_{28/3}Ti_{18}O_{54}$ composition showed properties of $\varepsilon_r = 93.2$, $Q\times f = 9770$ GHz, $\tau_f = +4.56$ ppm/°C when $x = 0.08$. In addition, there were many papers about properties and structure of impure BNT ceramics by other cations substituting for B-site ($Ti^{4+}$), such as $(Cr_{1/2}Nb_{1/2})^{4+}$ [14], $Al^{3+}$ [9], $(Mg_{1/3}Nb_{2/3})^{4+}$ [19] and so on.

All these works didn't investigate the relationship between structure of BNT ceramics and their microwave dielectric properties by using Raman spectroscopy. Raman spectrum analysis of BNT-(AN)$z$ ceramics would be momentous for BNT ceramics and set a model for the modified ceramic investigation.

## 2. Experimental procedures

### 2.1. Preparation of BNT-(AN)z

The starting raw powders: $BaCO_3$, $Al_2O_3$, $Nd_2O_3$ $Nb_2O_5$ and $TiO_2$ were high-purity (99.0%) powders and weighed according to the ratio of $Ba_{3.75}Nd_{9.5}Ti_{18-z}(Al_{1/2}Nb_{1/2})_zO_{54}$ (BNT-(AN)$z$) where z = 0, 0.5, 1.0, 1.5, 2.0, 2.5, 3.0. And milled in plastic jars using deionized water for 8 h. The resulting mixtures were calcined at 1100 °C for 5 h in air with 5°C/min heating rate. Then these calcined powders were produced with 7 wt% of a 10% solution of PVA added in the size of 15 mm in diameter and 8 mm in thickness under the pressure of 200 kg/cm$^2$. At last, the samples were preheated at 600 °C for 3 h to exclude the organic binder, and sintered at 1350–1425 °C for 4 h in air.

### 2.2. Characterization

After sintering completely, the bulk densities of samples were measured by the Archimedes method. The crystalline phases of the samples were determined with XRD using CuK<alpha> radiation (Philips x'pert Pro MPD, Netherlands). The visualization of crystal structure of ceramics was acquired by VESTA software with ceramics crystallography data [20]. The refinement of crystal unit cell parameters of samples was calculated by analyzing XRD data using the "Material Analysis Using Diffraction" (MAUD) based on the Rietveld method [21,22]. The microstructure of the samples was investigated by scanning electron microscopy(SEM) (FEI Inspect F, United Kingdom) coupled with energy dispersive spectrometer(-EDS) which detected the main chemical composition of specimens. Raman spectra of the samples were measured on Nicolet ALMEGA Raman spectrometer with the existing line at 523 nm of a Nd/YAG laser at room temperature, and collected in the range of 100–1000 cm$^{-1}$. The dielectric characteristics at microwave frequencies were measured by the Hakki–Coleman dielectric resonator method in the TE011 mode using a network analyzer (Agilent Technologies HP83752A) and a temperature chamber (DELTA 9023, Delta Design, USA). The temperature coefficient of resonant frequency ($\tau_f$) of specimens was determined from the difference between the resonant frequency (2 ~ 3 GHz) obtained at 25 °C and 85 °C using Eq. (1):

$$\tau_f = \frac{\Delta f}{f_0 \cdot \Delta t} \times 10^6 = \frac{f_{85°C} - f_{25°C}}{f_{25°C} \times (85-25)} \times 10^6 \ (\text{ppm}/°\text{C}) \quad (1)$$

In Eq. (1), $f_{25\ °C}$ and $f_{85\ °C}$ represent the resonant frequency at 80 °C and 25 °C, respectively. All cylindrical samples were untreated after sintering when they were made to do dielectric measurements.

## 3. Results and discussion

### 3.1. Crystalline structure and microstructure

The X-ray diffractograms of BNT-(AN)$z$ ($z = 0$–3) ceramics sintered at 1375 °C for 4 h in air are shown in Fig. 2 (a). All samples were crystalized as a tungsten-bronze type like structure phase $BaNd_2Ti_5O_{14}$ (JCPDS No. 33–0166) and no peaks for secondary phase were detected, which implied that it did form a single phase and composite ions $(Al_{1/2}Nb_{1/2})^{4+}$ had entered into crystal cell. Furthermore, Fig. 2 (b) depicts that the diffraction peaks of all samples shift towards the higher angle with the increase of $z$ value. The intensity of the splitting peak (as shown in Fig. 2 (b)) gradually increased when $z$ value increased 0 to 3. We can see from the XRD patterns of the JCPDS No. 33–0166 in Fig. 2 (a), the strongest diffraction peak of (151) face ($2\theta = 31.57°$) was very close to diffraction peak (270) face ($2\theta = 31.63°$). So the splitting peak

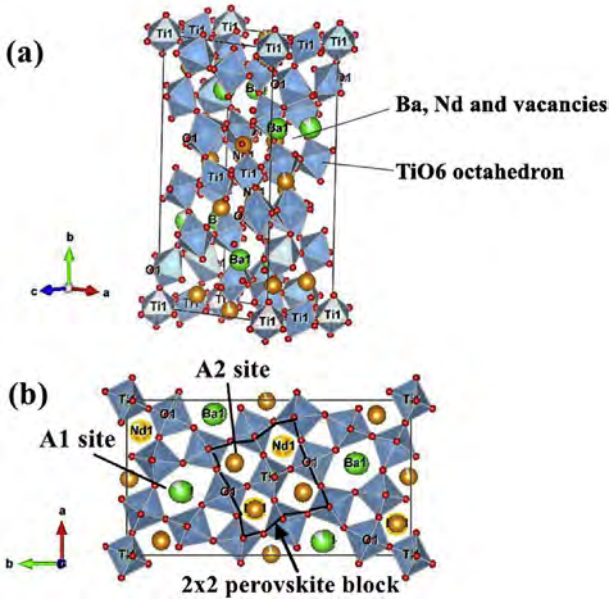


**Fig. 1.** Schematic representation of (a) $Ba_{3.75}Nd_{9.5}Ti_{18}O_{54}$ with tungsten-bronze type like structure and (b) the c-axis was chosen as the short axis.

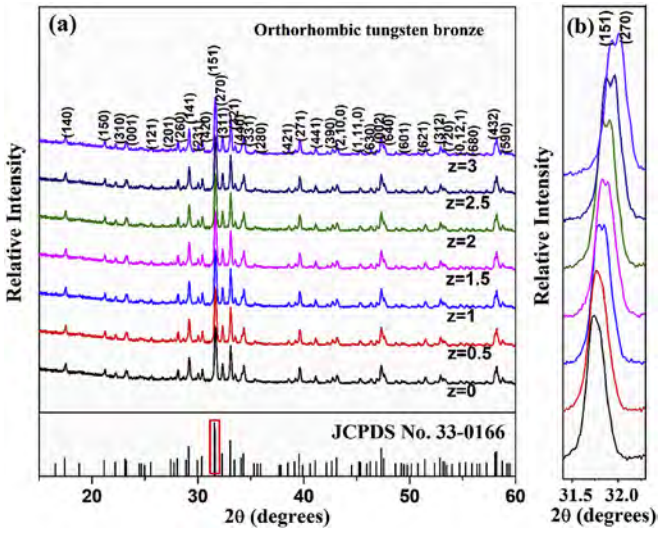


**Fig. 2.** (a) XRD patterns of BNT-(AN)$z$ ($z = 0$–3) ceramics sintered at 1375 °C for 4 h in air. (b) The characteristic peaks of (270) and (151) for BNT-(AN)$z$ phase of corresponding samples.

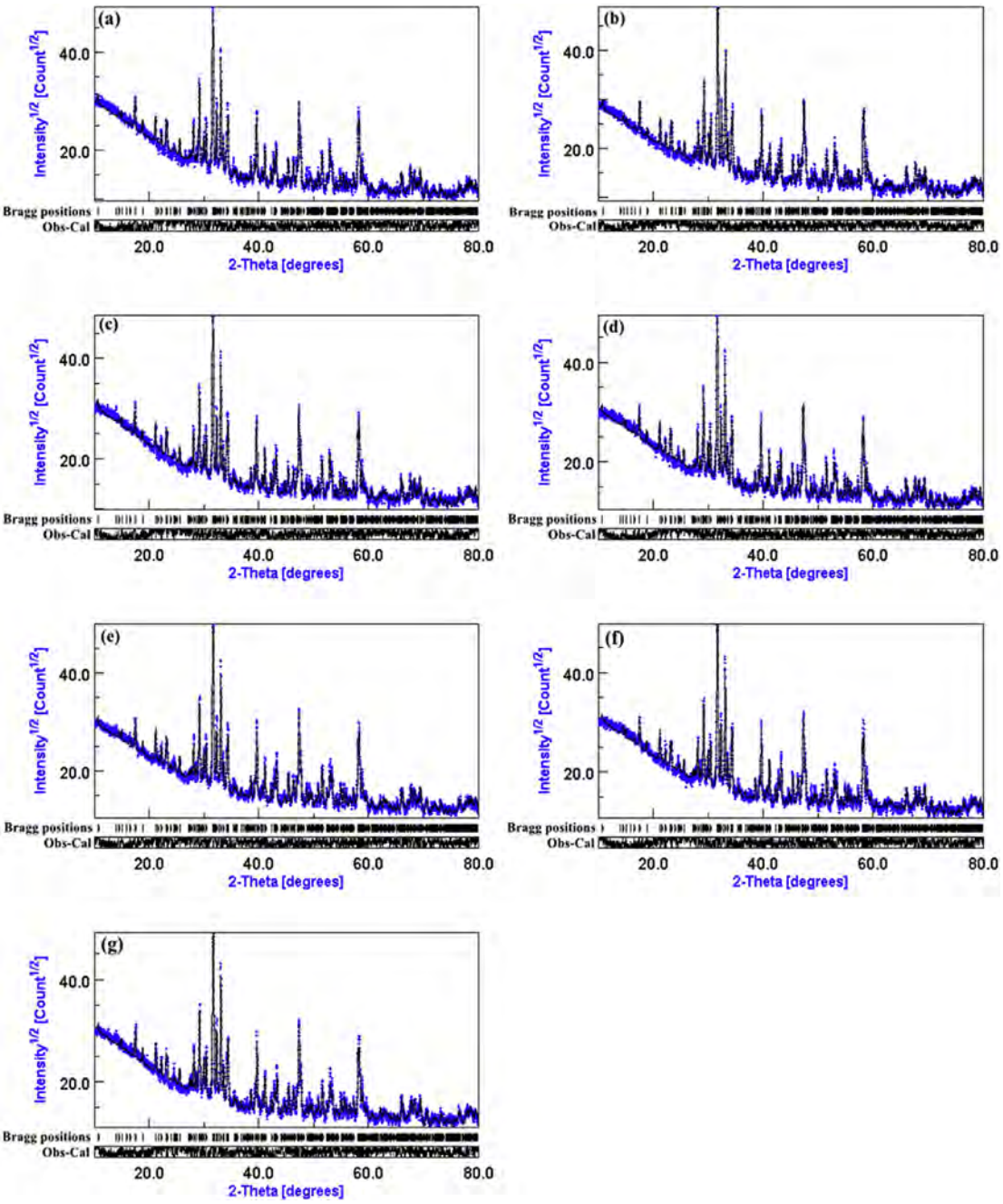


**Fig. 3.** Experimental (blue cross) and calculated (black line) X-ray powder diffraction profiles for BNT-(AN)$z$ ceramics sintered at 1375 °C for 4 h with (a) $z = 0$; (b) $z = 0.5$; (c) $z = 1$; (d) $z = 1.5$; (e) $z = 2$; (f) $z = 2.5$; (g) $z = 3$; The short vertical lines below the patterns mark the positions of Bragg reflections. The bottom continuous line is the difference between the observed and the calculated intensity. (For interpretation of the references to colour in this figure legend, the reader is referred to the web version of this article.)

suggested that the diffracted intensity of (270) face increased when $(Al_{1/2}Nb_{1/2})^{4+}$ substituted for $Ti^{4+}$ in BNT ceramics, and further studies were required to confirm this finding. In order to further investigate the shift of the diffraction peaks and effect of the substitution of $(Al_{1/2}Nb_{1/2})^{4+}$ on crystallographic parameters, the Rietveld refinement method were carried out on the basis of the X-ray diffraction data of all sintered samples. As shown in Fig. 3, the crystalline structure of all $(Al_{1/2}Nb_{1/2})^{4+}$ doped BNT ceramics sintered at 1375 °C for 4 h was defined as tungsten-bronze type like structure in *Pbam* space group (No. 55) by comparison between experimental and calculated X-ray diffraction patterns with the Rietveld refinement methods. In addition, the Rietveld discrepancy factors R values [22] and the refined crystallographic parameters of all samples are presented in Table 1. With the variety of $z$ values, crystallographic parameters values decreased from $a$ = 12.18-3437 Å, $b$ = 22.32194 Å, $c$ = 3.8431513 Å, to $a$ = 12.173024 Å, $b$ = 22.221062 Å, $c$ = 3.8325378 Å, and the unit cell volume also decreased from $V$ = 1045.175548 Å$^3$ to $V$ = 1036.691974 Å$^3$. The average ion radii of $Nb^{5+}$ (0.64 Å) and $Al^{3+}$ (0.535 Å) is 0.5875 Å, which is less than the ion radii of $Ti^{4+}$ (0.605 Å). So it was inevitable to decrease the lattice parameters, and the diffraction peaks moved towards the high angle based on Bragg's law ($2d\sin\theta = n\lambda$) when composite ions $(Al_{1/2}Nb_{1/2})^{4+}$ substituted for $Ti^{4+}$ [23]. The shift of diffraction peak was consistent with changing of lattice parameters

**Table 1**
Refined crystal unit cell parameters, R values, Packing fraction and theoretical dielectric constant versus composition in BNT-(AN)*z* ($z = 0–3$) ceramics sintered at 1375 °C for 4 h in air (R*w*: weight profile; R*wnb*: a value similar to that reported for single-crystal refinements; R*b*; the Bragg-intensity R value; R*exp*: excepted weighted profile factor).

| *z* (mol) | 0 | 0.5 | 1 | 1.5 | 2 | 2.5 | 3 |
|---|---|---|---|---|---|---|---|
| *a* (Å) | 12.183437 | 12.187622 | 12.182518 | 12.179743 | 12.176989 | 12.175154 | 12.173024 |
| *b* (Å) | 22.32194 | 22.285225 | 22.263275 | 22.254554 | 22.249706 | 22.236445 | 22.221062 |
| *c* (Å) | 3.8431513 | 3.8405956 | 3.8375553 | 3.8358342 | 3.834707 | 3.8337325 | 3.8325378 |
| *V* (Å$^3$) | 1045.175548 | 1043.120737 | 1040.832296 | 1039.721074 | 1038.954137 | 1037.914613 | 1036.691974 |
| *Rw* (%) | 8.704771 | 6.7181716 | 8.139981 | 7.5027847 | 8.414023 | 8.305101 | 8.65078 |
| *Rwnb* (%) | 10.085603 | 5.9232564 | 9.090537 | 7.682213 | 10.858708 | 10.00458 | 10.864566 |
| *Rb* (%) | 6.882318 | 5.2402325 | 6.4687734 | 5.9197803 | 6.433322 | 6.503445 | 6.7127643 |
| *Rexp* (%) | 5.561764 | 5.666339 | 5.4596744 | 5.4100113 | 5.330454 | 5.2767596 | 5.299943 |
| Packing fraction (%) | 70.48465 | 70.56948 | 70.75091 | 70.76540 | 70.90624 | 70.56047 | 70.34915 |
| $\varepsilon_{r(the)}$ | 85.96 | 83.80 | 81.97 | 78.98 | 75.86 | 73.21 | 70.86 |

and this suggested that BNT-(AN)*z* crystallized into orthorhombic tungsten bronze *Pbam* structure.

The appearance of single phase of all samples could be clarified by considering the linear variation of tolerance factor with different *z* values, which is shown in Fig. 4. Shannon and Ubic et al. [5,24] have reported that the tolerance factor of $Ba_{6-3x}Nd_{8+2x}Ti_{18}O_{54}$ solid solution can be calculated by Eq. (2):

$$t = \frac{\frac{4+x}{5}R_{Nd^{3+}} + \frac{1-x}{5}R_{Ba^{2+}} + R_{O^{2-}}}{\sqrt{2}\left[\frac{18-z}{18}R_{Ti^{4+}} + \frac{z}{18}\left(\frac{1}{2}R_{Al^{3+}} + \frac{1}{2}R_{Nb^{5+}}\right) + R_{O^{2-}}\right]} \quad (2)$$

Here, $R^{2+}_{Ba}$, $R^{3+}_{Nd}$, $R^{4+}_{Ti}$, $R^{3+}_{Al}$, $R^{5+}_{Nb}$ and $R^{2-}_{O}$ signify the ionic radii of $Ba^{2+}$, $Nd^{3+}$, $Ti^{4+}$, $Al^{3+}$, $Nb^{5+}$and $O^{2-}$ respectively. The linear increase of tolerance factor in tungsten-bronze type like structure implied a more stable system [25].

Fig. 5 presents evolution of microstructure of BNT-(AN)*z* ceramics ($z = 0–3$) sintered at 1375 °C for 4 h. It was clear that the typical columnar grains could be observed for all composition and independently, and this indicated that the tungsten bronze phase structure did exist, which was consistent with the XRD results. As we can see, the grain size gradually decreased with increase of contents of composite ions $(Al_{1/2}Nb_{1/2})^{4+}$, and heterogeneity of grain size was observed in BNT-(AN)2.5 and BNT-(AN)3 ceramics (Fig. 5(f and g)). Meanwhile, data of EDS analysis were exhibited in Fig. 6 to identify the phase element constitution. According to the EDS of grain A, B and C, the ratios of Ba:Nd:(Ti+$(Al_{1/2}Nb_{1/2})$) were close to 1: 2: 5, and this powerfully proved that $(Al_{1/2}Nb_{1/2})^{4+}$ successfully substituted for $Ti^{4+}$ at B site. Moreover, morphology features of BNT-(AN)2 ceramics sintered at different temperature are shown in Fig. 7. The grain size became heterogeneous and grain boundary became blurry with increasing temperature.

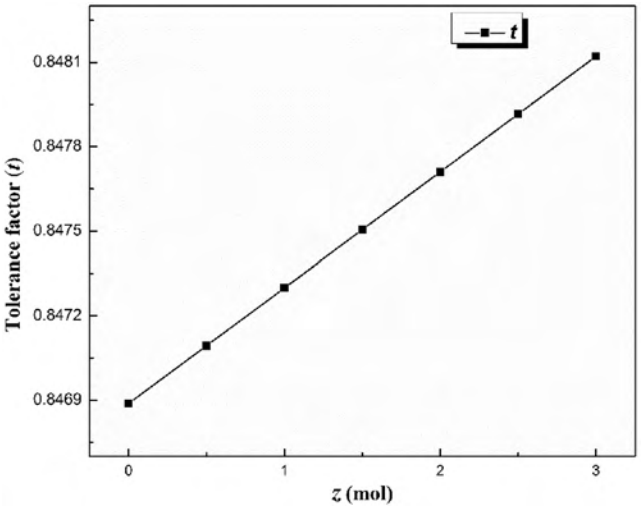


**Fig. 4.** Theoretical tolerance factor (*t*) of BNT-(AN)*z* ceramics sintered at 1375 °C for 4 h with (a) $z = 0$; (b) $z = 0.5$; (c) $z = 1$; (d) $z = 1.5$; (e) $z = 2$; (f) $z = 2.5$; (g) $z = 3$.

### 3.2. Raman spectra study

Raman spectroscopy is one of the powerful techniques for analysis of physical properties of oxygen octahedra and its arrangement [26]. Factor group symmetry analysis method was applied to analyze the lattice vibration of BNT crystal. The BNT crystal belonged to the space group *Pbam*, and had a symmetric center. As is well known, the vibration spectrum of a crystal with N atoms in the unit cell is made up of 3N branches. Accordingly, 86 atom sites in the unit cell of tungsten–bronze structured BNT fundamental lattice give rise to 258 branches. These modes could be characterized using group theoretical method according to the $D_{2h}$ space group. The irreducible representations for the lattice were obtained using the data given in Table 2 and the following equation [27]:

$$n_m = \frac{1}{h}\sum_R \chi(R)U(R)(\pm 1 + 2cos\theta_R) \quad (3)$$

where $n_m$ is the number of vibrational modes with a symmetry presented by the *m*th irreducible representation; $h = 8$ is the order of a group G made up of all symmetry elements *R*; $\chi(R)$ is elements *R*'s character of reducible representation; $U(R)$ is the number of atoms that are invariant under the symmetry operations of the group; represents the symmetric transition; and $(\pm 1 + 2\cos\theta_R)$ is the sum of elements on the diagonal of the matrix R, namely, the trace of the matrix.

Finally, all vibrations were determined: total vibrational modes were $40A_g + 23A_u + 40B_{1g} + 23B_{1u} + 20B_{2g} + 46B_{2u} + 20B_{3g} + 46B_{3u}$. $B_{1u} + B_{2u} + B_{3u}$ modes were acoustic; $22B_{1u} + 45B_{2u} + 45B_{3u}$ modes were Infrared active; and $40A_g + 40B_{1g} + 20B_{2g} + 20B_{3g}$ modes were Raman active. According to factor group analysis, 126 vibrational modes were Raman active whereas we observed directly maximum 12 Raman modes in BNT-(AN)*z* ceramics sintered at 1375 °C for 4 h, which were shown in Fig. 8. This discrepancy was quite possible due to the net change in the polarizability, or dipole moment of the vibrational mode may not be strong enough to give rise to observable Raman modes [28].

Nine changes of modes of vibration with changes of *z* value were marked using dotted line in Fig. 8. Types of vibrational modes and positions of these modes for BNT-(AN)*z* ceramics were given in Table 3. The frequencies of these peaks match well with the previous work [29–31]. The oxygen octahedra were tilting in BNT-(AN)*z* ceramics structure (as shown in Fig. 1) compared to the perovskite structure, and Raman spectra of BNT-(AN)*z* ceramics were be similar to Raman spectra of $CaTiO_3$ ceramics [32,33]. From ref.

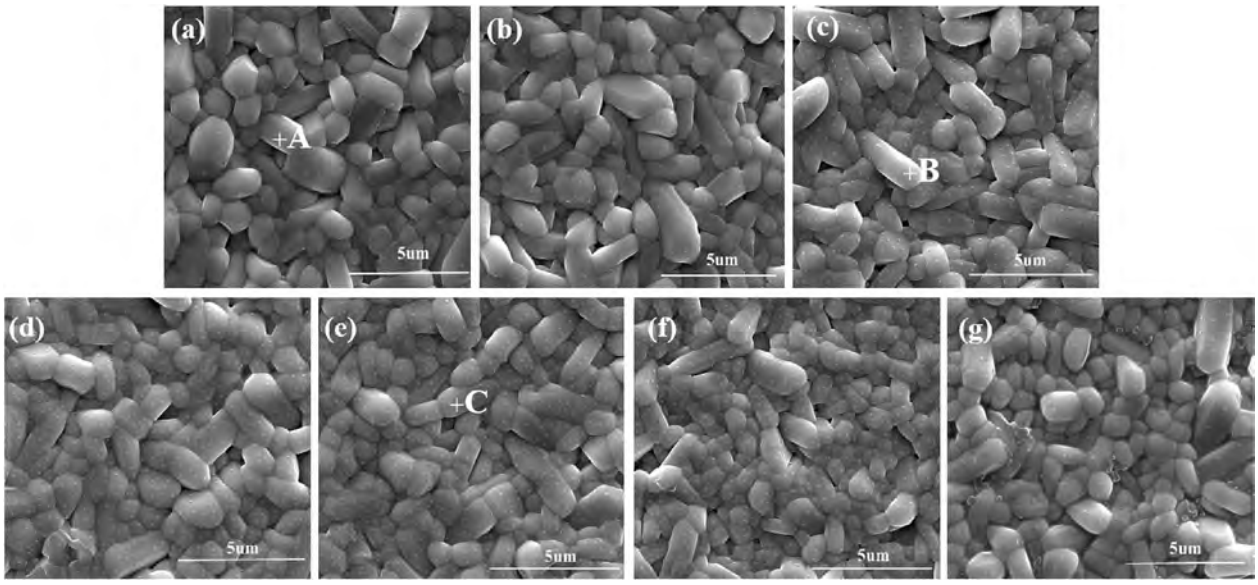


**Fig. 5.** SEM photographs of BNT-(AN)$z$ ceramics sintered at 1375 °C for 4 h with (a) $z = 0$; (b) $z = 0.5$; (c) $z = 1$; (d) $z = 1.5$; (e) $z = 2$; (f) $z = 2.5$; (g) $z = 3$.

29–33, the Raman bands at 753.2 $cm^{-1}$, 590.0 $cm^{-1}$ and 530.2 $cm^{-1}$ were associated with the Ti–O symmetric stretching vibration. The 404.4 $cm^{-1}$ band was assigned to the Ti–O bending vibration. The bands between 200 $cm^{-1}$ to 300 $cm^{-1}$ were attributable to the rotation of the oxygen cage, and the bands in the region 100–200 $cm^{-1}$ were associated with the translation of cation ($Nd^{3+}$ and $Ba^{2+}$) in the A site. The bands at 753.2 $cm^{-1}$, 590.0 $cm^{-1}$ and 530.2 $cm^{-1}$ were determined to be $A_g$, $B_{1g}$ and $A_g$ respectively. Fig. 8(a) illustrated that as $z$ ($(Al_{1/2}Nb_{1/2})^{4+}$concentration) increased, the bands at 590.0 $cm^{-1}$, 530.2 $cm^{-1}$ and 404.4 $cm^{-1}$ became broad presumably due to a reduction in the degree of B site order [33]. As the $Ti^{4+}$, $Al^{3+}$ and $Nb^{5+}$ were distributed throughout the B sites, there was therefore a distribution of phonon frequencies, resulting in a broad band, characteristic of "disordering" type. Moreover, the bands at 232.9 $cm^{-1}$ and 277.8 $cm^{-1}$ became broad obviously (as shown in Fig. 8(b)), which indicated that vibration associated with the rotation of oxygen cage became weaker as $z$ increased. This confirmed that flexible oxygen octahedra networks became stressed-rigid [27,34]. The Raman bands in the region 100–200 $cm^{-1}$ presented the obvious variety of intensity and width in BNT-(AN)$z$ ceramics, especially in the region 100–150 $cm^{-1}$. This was perhaps owing to lattice distortion caused by decrease of the unit cell volume [27], and the vibration caused by $Ba^{2+}$ and $Nd^{3+}$ was restricted in stressed-rigid oxygen octahedra networks. In addition, it was considered that local structural changes resulted in such significant changes when the substitution of $(Al_{1/2}Nb_{1/2})^{4+}$ increased. The B sites were considered to be occupied randomly by $Ti^{4+}$, $Al^{3+}$ and $Nb^{5+}$ in BNT-(AN)$z$ ceramics structure. Due to different ionic sizes and force constants of $Ti^{4+}$, $Al^{3+}$ and $Nb^{5+}$, two adjacent corner sharing oxygen octahedra may become nonequivalent. If octahedra were not equivalent, the constituent oxygen atoms occurred in the local positions without an inversion center and their vibrations became Raman active. This mode was a simple motion of the oxygen atoms like the breathing-type mode of a free oxygen octahedron ions [35]. So significant changes of some Raman bands (100–150 $cm^{-1}$) could be explained by $Al^{3+}$ and $Nb^{5+}$ occupational disorder and the octahedral distortion, subsequently oxygen octahedra became more tilted [36]. The blue shift of Raman bands (753.2 $cm^{-1}$, 530.2 $cm^{-1}$, 277.8 $cm^{-1}$, 232.9 $cm^{-1}$, 112.8 $cm^{-1}$) proved that unit cell volume decreased when the substitution of $(Al_{1/2}Nb_{1/2})^{4+}$ increased.

### 3.3. Dielectric properties

Relative densities and microwave dielectric properties of BNT-(AN)$z$ ceramics sintered at different temperature are plotted as

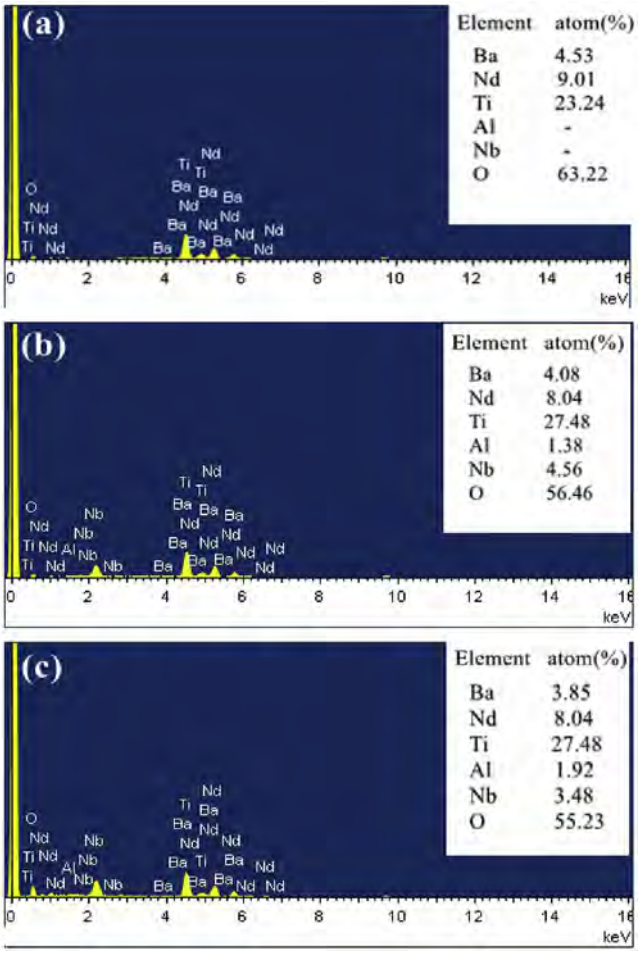


**Fig. 6.** EDS analysis of BNT-(AN)$z$ ceramics sintered at 1375 °C for 4 h with (a) grain A; (b) grain B; (c) grain C in Fig. 5.

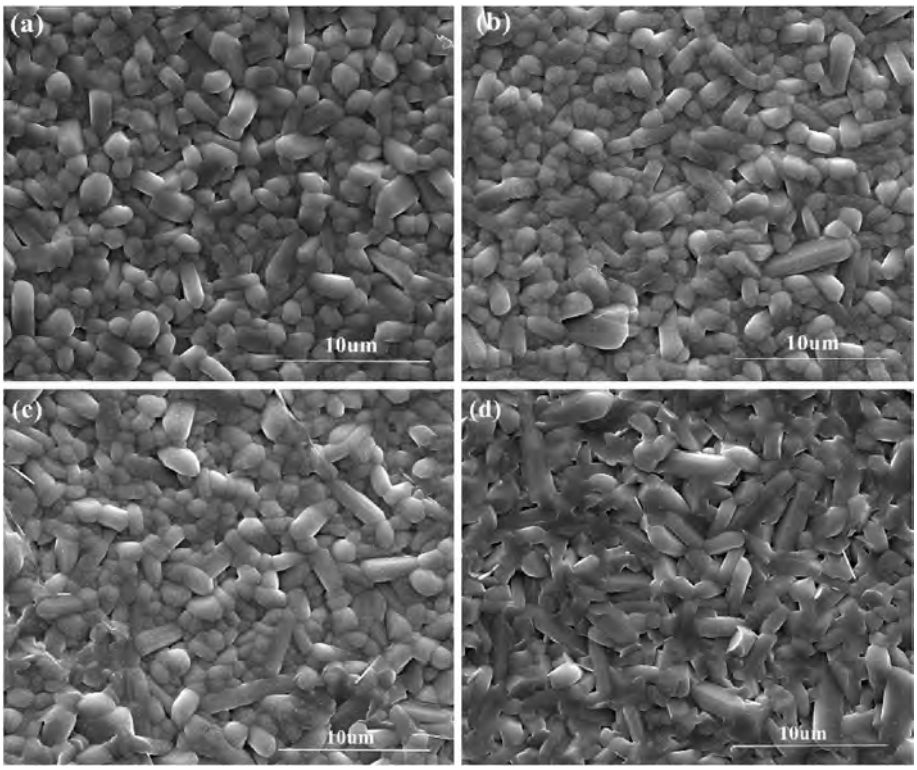


**Fig. 7.** SEM photographs of BNT-(AN)2 ceramics sintered at different temperature for 4 h with (a) 1350 °C; (b) 1375 °C; (c) 1400 °C; (d) 1425 °C.

function of composition $z$ in Fig. 9. As presented in Fig. 9 (a), relative densities of all samples were higher than 96%, and increased firstly as concentration of composite ions $(Al_{1/2}Nb_{1/2})^{4+}$ increased, and then decreased. Pores were observed in Figs. 5 and 7, which indicate that it was possible to reach the 100% relative density for ceramics by different sintering schedule. BNT-(AN)2 ceramics sintered at 1375 °C showed the highest relative density of 98.5%. The addition of $(Al_{1/2}Nb_{1/2})^{4+}$ could improve the densification of BNT-(AN)$z$ ceramics partly.

Fig. 9 (b) shows the $Q\times f$ value of BNT-(AN)$z$ ceramics sintered at different temperatures and the packing fraction of BNT-(AN)$z$ ceramics sintered at 1375 °C as a function of $z$ value. The high $Q\times f$ value of BNT-(AN)$z$ ceramics sintered at 1375 °C was obtained compared with the other compositions, and it was greatly improved from 9277 GHz at $z = 0$ to 13,177 GHz at $z = 2$. This tendency was similar with the relative density because of densification process. Generally, not only relative density could affect the dielectric loss, but also cation ordering, impurity secondary phase as well as packing fraction [22,37]. In this work, the packing fraction was calculated using Eq. (4) to find out the relationship between intrinsic loss with $Q\times f$ value of ceramics, which was based on the fact that changing $Q\times f$ value of ceramics is independent of relative density greater than 96% [22,38–40]. Packing fraction data of BNT-(AN)$z$ ceramics sintered at 1375 °C were listed in Table 1 and inset Fig. 9 (b). Obviously, the packing fraction and $Q\times f$ value both reached the maximum value of 70.91% and 13,177 GHz at $z = 2$, then decreased when the content of $(Al_{1/2}Nb_{1/2})^{4+}$ substitution increased. Furthermore, the substitution of the three-valence element Al for the four-valence element Ti restrained the $Ti^{3+}$ accumulation by this reaction: $Al_2O_3 \xrightarrow{TiO_2} 2Al'_{Ti} + V_O^{\bullet\bullet} + 3O_O^x$ [41]. In addition, more homogeneous grains were observed in Fig. 5(b–e), which was conducive to the densification and improvement of $Q\times f$ value [42]. But the appearance of abnormal grains in BNT-(AN)2.5 and BNT-(AN)3 ceramics (Fig. 5 (f, g)) deteriorated the quality factor. What's more, the changes of packing fraction were corresponding to the variation of relative density as the $z$ value increased from 0 to 3.

$$\text{Packing fraction } (\%) = \frac{volume\ of\ packed\ ions}{volume\ of\ unit\ cell} \times Z = \frac{\frac{4}{3}\pi \times \left[r_{Ba}^3 \times 1 + r_{Nd}^3 \times 2 + r_{Ti}^3 \times \left(\frac{18-z}{18}\right) \times 5 + \frac{5}{18} \times \frac{z}{2} \times \left(r_{Al}^3 + r_{Nb}^3\right) + r_O^3 \times 14\right]}{V_{cell}} \times 4 \quad (4)$$

Fig. 9 (c) depicts the dielectric constant of BNT-(AN)$z$ ceramics sintered at 1350 °C, 1375 °C, 1400 °C, 1425 °C for 4 h. The optimum sintering temperature of BNT-(AN)$z$ ceramics could be determined at the 1375 °C, at which relative density reached higher values than the other temperature. The $\varepsilon_r$ decreased from 84.6 to 70.3. Usually the dielectric constant had no obvious relationship with the high relative density (higher than 96%) [22,40]. Many studies have reported that dielectric polarizabilities had a considerable influence on the dielectric constant [9,14,43]. According to the Clausius-

**Table 2**
Data used for irreducible representation analysis.

| $D_{2h}$ | R | | | | | | | |
|---|---|---|---|---|---|---|---|---|
| | E | $C_2^z$ | $C_2^y$ | $C_2^x$ | I | $\sigma_z$ | $\sigma_y$ | $\sigma_x$ |
| $A_g$ | 1 | 1 | 1 | 1 | 1 | 1 | 1 | 1 |
| $B_{1g}$ | 1 | 1 | −1 | −1 | 1 | 1 | −1 | −1 |
| $B_{2g}$ | 1 | −1 | 1 | −1 | 1 | −1 | 1 | −1 |
| $B_{3g}$ | 1 | −1 | −1 | 1 | 1 | −1 | −1 | 1 |
| $A_u$ | 1 | 1 | 1 | 1 | −1 | −1 | −1 | −1 |
| $B_{1u}$ | 1 | 1 | −1 | −1 | −1 | −1 | 1 | 1 |
| $B_{2u}$ | 1 | −1 | 1 | −1 | −1 | 1 | −1 | 1 |
| $B_{3u}$ | 1 | −1 | −1 | 1 | −1 | 1 | 1 | −1 |
| $U(R)$ | 86 | 6 | 0 | 0 | 6 | 86 | 0 | 0 |
| $\pm1 + 2\cos\theta_R$ | 3 | −1 | −1 | −1 | −3 | 1 | 1 | 1 |

Mosotti equation, the dielectric polarizability was calculated by Eq. (5):

$$\alpha_D = \frac{V_m(\varepsilon_r - 1)}{b(\varepsilon_r + 2)} \tag{5}$$

where $\varepsilon_r$ is the theoretical dielectric constant; $V_m$ is the molar volume; $\alpha_D$ is the theoretical dielectric polarizability; b has the

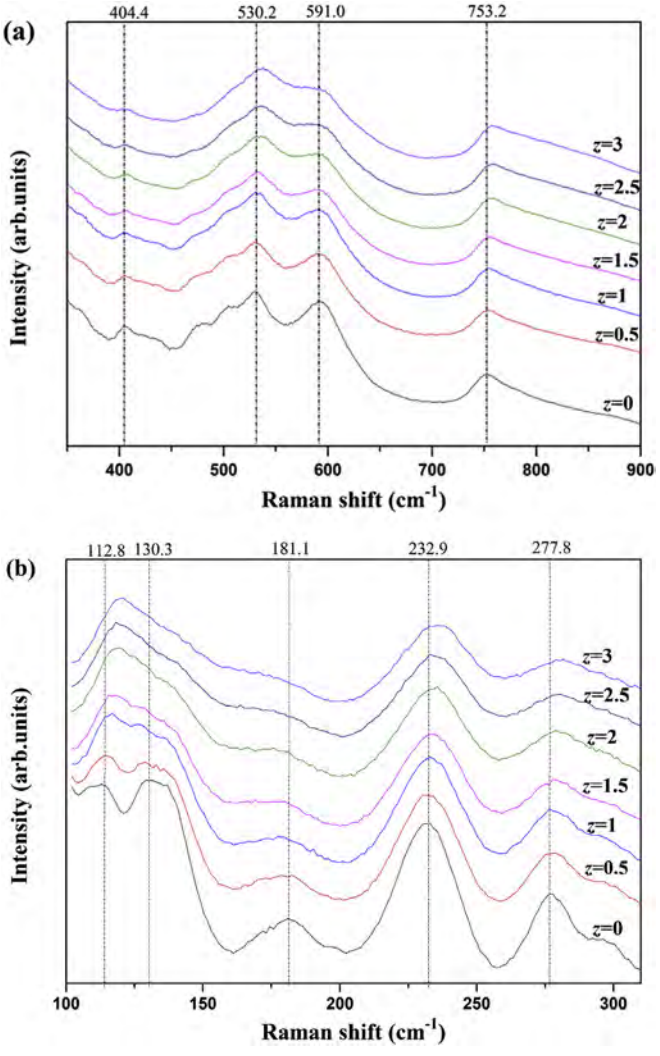


**Fig. 8.** Raman spectra of BNT-(AN)$z$ ceramics sintered at 1375 °C for 4 h: (a) 400–900 $cm^{-1}$; (b) 100–310 $cm^{-1}$.

**Table 3**
Raman active modes and Raman shift observed for BNT-(AN)$z$ ceramics.

| Raman active modes | Raman shift ($cm^{-1}$) | | | | | | |
|---|---|---|---|---|---|---|---|
| | $z = 0$ | $z = 0.5$. | $z = 1$ | $z = 1.5$ | $z = 2$ | $z = 2.5$ | $z = 3$ |
| $A_g$ | 753.2 | 755.6 | 756.4 | 757.1 | 757.8 | 758.4 | 759.3 |
| $B_{1g}$ | 591.0 | 592.2 | 591.0 | 591.7 | 591.0 | 590.4 | 591.0 |
| $A_g$ | 530.2 | 531.4 | 532.4 | 533.7 | 536.1 | 537.7 | 539.2 |
| Unknown | 404.4 | 403.1 | 403.1 | 403.1 | 403.1 | 403.1 | 403.1 |
| Unknown | 277.8 | 279.1 | 280.2 | 280.9 | 281.6 | 282.5 | 286.8 |
| Unknown | 232.9 | 232.9 | 231.6 | 232.9 | 233.7 | 234.4 | 235.6 |
| Unknown | 181.1 | 182.4 | 181.6 | 181.1 | – | – | – |
| Unknown | 130.3 | 128.9 | 128.9 | – | – | – | – |
| Unknown | 112.8 | 114.1 | 115.8. | 116.2 | 117.9 | 118.4 | 119.5 |

value of $4\pi/3$. The theoretical dielectric constant ($\varepsilon_{r(the)}$) of samples sintered at 1375 °C for 4 h was calculated in Table 1 and shown in the embedded figure in Fig. 9 (c). The $\varepsilon_r$ and $\varepsilon_{r(the)}$ of samples both decreased with increase of $z$ value because of lower dielectric polarizability of $(Al_{1/2}Nb_{1/2})^{4+}$ (2.38 Å$^3$) comparing to $Ti^{4+}$ (2.93 Å$^3$) [14,24].

Fig. 9 (d) shows the trend of $\tau_f$ of BNT-(AN)$z$ ($z = 0$–3) ceramics sintered at 1375 °C for 4 h varies with sintering temperature. Distinctly, $\tau_f$ of BNT-(AN)$z$ ($z = 0$–3) ceramics decreased towards the direction of the negative value when the concentration of the substitution of $(Al_{1/2}Nb_{1/2})^{4+}$ increased. It was reported that the $\tau_f$ of $Ba_{6-3x}Nd_{8+2x}Ti_{18}O_{54}$ ceramics was dependent on the tilting of oxygen octahedra [8, 44, 45], and oxygen octahedra were necessarily bound up with the B site bond valence ($S_i$). From bond-valence model, The bond valence of B site atom in oxygen octahedra was calculated using Eq. (6) and (7) [46, 47].

$$s_{ij} = \exp\left(\frac{R_{ij} - d_{ij}}{B}\right) \tag{6}$$

$$S_i = \sum_j s_{ij} \tag{7}$$

where $R_{ij}$ is the bond valence parameter, which has been tabulated based on plenty of experiment data, $d_{ij}$ is the length of a bond between atom i and j, and B is an empirically determined universal constant with a value of 0.37. Table 4 summarizes the bond valence of B site and $\tau_f$ values of BNT-(AN)$z$ ($z = 0$–3) ceramics sintered at 1375 °C for 4 h. We could see that the bond valence of B site enhanced with increase of $z$ value and consequently, the $\tau_f$ value decreased from +63.6 ppm/°C to −8.9 ppm/°C. This could be explained by stronger bond strength between oxygen and B-site ion with larger bond valence [48]. Furthermore, the $\tau_f$ was related to the temperature coefficient of dielectric constant ($\tau_\varepsilon$) and the thermal expansion coefficient ($\alpha_L$), as given in Eq. (8).

$$\tau_f = -\left(\frac{\tau_\varepsilon}{2} + \alpha_L\right) \tag{8}$$

Here, $\alpha_L$ is commonly a positive constant in ceramics. So, the $\tau_f$ value was directly determined by $\tau_\varepsilon$. Colla et al. [49]. Derived an expression for $\tau_\varepsilon$ as Eq. (9).

$$\tau_\varepsilon = \frac{(\varepsilon - 1)(\varepsilon + 2)}{\varepsilon}\left[\frac{1}{\alpha_m}\left(\frac{\partial \alpha_m}{\partial T}\right)_V + \frac{1}{\alpha_m}\left(\frac{\partial \alpha_m}{\partial V}\right)_T\left(\frac{\partial V}{\partial T}\right)_P - \frac{1}{V}\left(\frac{\partial V}{\partial T}\right)_P\right] \tag{9}$$

where $\alpha_m$ and $V$ denote the polarizability and volume, respectively. The first term in the bracket in Eq. (9) normally has negative value. For tilting octahedra structure, the second and third terms are normally the largest ones and $\tau_\varepsilon$ depends mainly on them. In BNT-

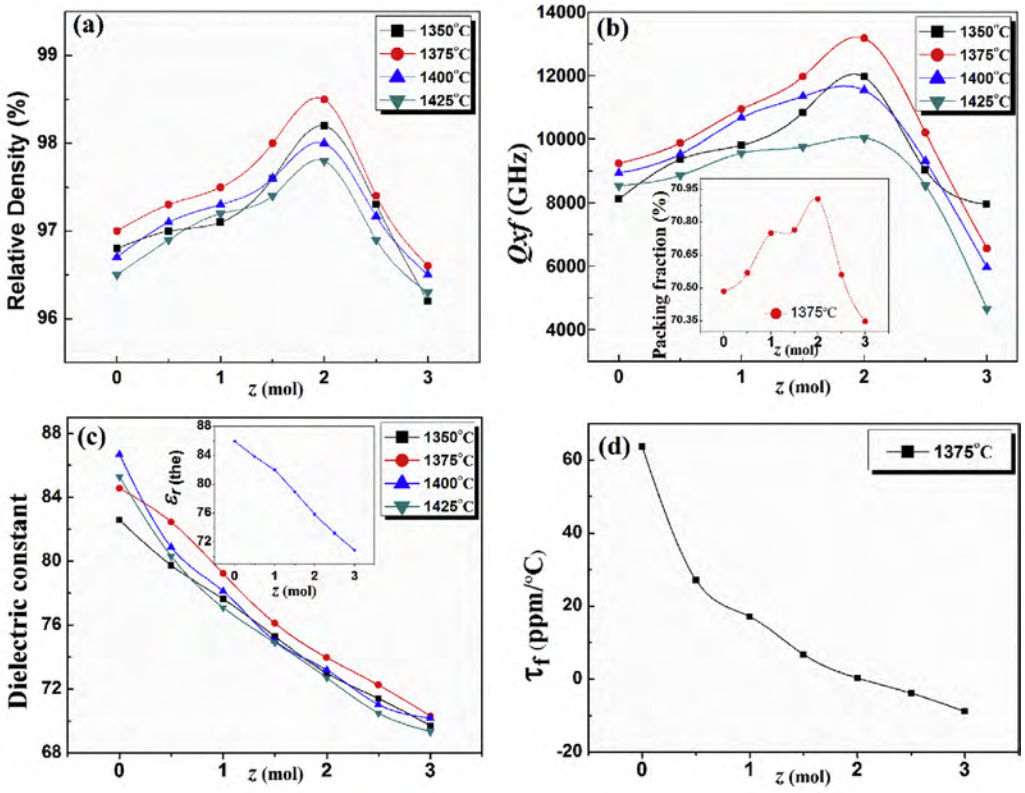


**Fig. 9.** Relative densities and microwave dielectric properties of BNT-(AN)$z$ ceramics sintered at 1350 °C, 1375 °C, 1400 °C, 1425 °C for 4 h with (a) relative density; (b) $Q\times f$ value; (c) dielectric constant (d) temperature coefficient of resonant frequency ($\tau_f$).

**Table 4**
Bond valence of B site and $\tau_f$ values of BNT-(AN)$z$ ($z = 0$–3) ceramics sintered at 1375 °C for 4 h.

| $z$ (mol) | 0 | 0.5 | 1 | 1.5 | 2 | 2.5 | 3 |
|---|---|---|---|---|---|---|---|
| $R_{B\text{-}O}$ | 1.815 | 1.8140556 | 1.8131111 | 1.8121667 | 1.8112222 | 1.8102778 | 1.8093333 |
| $d_{B\text{-}O}$ | 1.869315 | 1.86812041 | 1.8667533 | 1.8660887 | 1.86562978 | 1.8650074 | 1.864275 |
| $S_B$ | 5.172046 | 5.175012 | 5.17952 | 5.180394 | 5.184318 | 5.186319 | 5.19024 |
| $\tau_f$ (ppm/°C) | +63.6 | +27.2 | +17.1 | +6.7 | +0.3 | −3.9 | −8.9 |

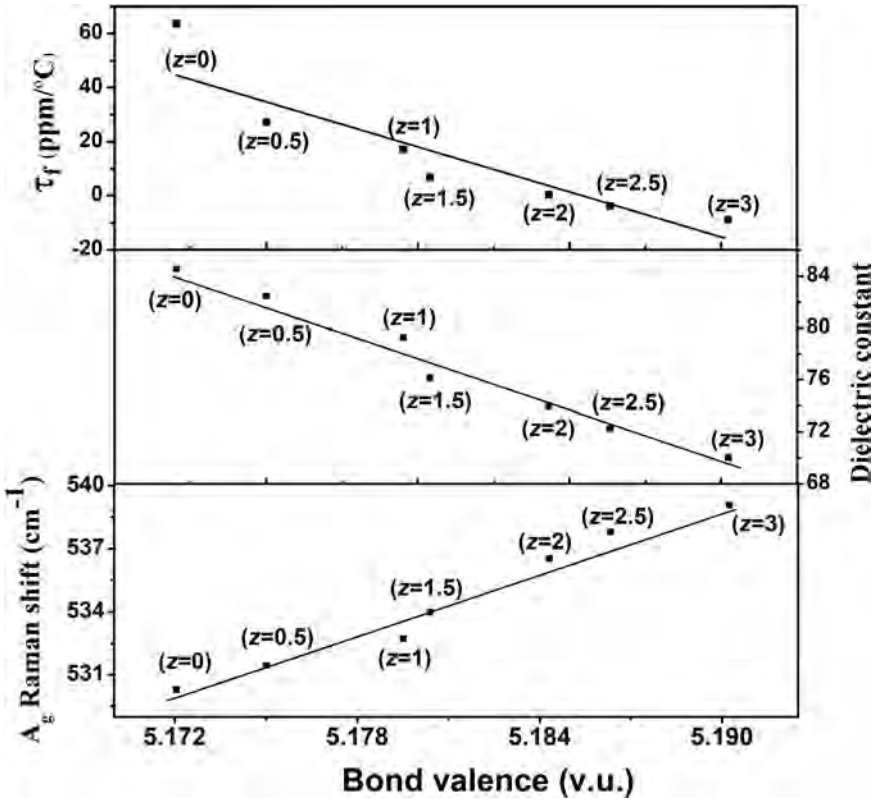


**Fig. 10.** Correlation between bond valence and Raman shift, dielectric constant and temperature coefficient of resonant frequency ($\tau_f$). The number in the bracket is $z$ value.

(AN)$z$ ceramics, the substitution of $(Al_{1/2}Nb_{1/2})^{4+}$ for $Ti^{4+}$ gave rise to the more distorted oxygen octahedra and tend to have near zero or positive $\tau_\varepsilon$ [44, 49], which corresponded to a decrease of the $\tau_f$ by Eq. (8). We obtained a near zero $\tau_f$ value of +0.3 ppm/°C BNT-(AN)$z$ ceramics with $z = 2$.

Fig. 10 depicts the trend of Raman shift, dielectric constant and $\tau_f$ with variation of bond valence. With increase of bond valence, Raman shift of $A_g$ mode increased, and dielectric constant and $\tau_f$ represented a declined trend. These trend were plotted as straight line in Fig. 10. According to Liao's study [27], the blue shift of Raman active modes (such as $A_g$ and $B_{1g}$) and bond valence of B site indicated that oxygen octahedra became stressed-rigid and more tilted, which have been discussed in the part of Raman spectra study, and manifested the unit cell volume decreased in BNT-(AN)$z$ ceramics with increase of the concentration of $(Al_{1/2}Nb_{1/2})^{4+}$. As a result, dielectric constant and $\tau_f$ value decreased.

## 4. Conclusions

The BNT-(AN)$z$ ceramics were synthesized by conventional solid state reaction method. XRD patterns of BNT-(AN)$z$ ($z$ = 0–3) ceramics showed that all samples were crystalized as a tungsten-bronze type like structure phase, and typical columnar grains were observed in SEM photographs. The EDS analysis of grains (A, B and C) powerfully proved that $(Al_{1/2}Nb_{1/2})^{4+}$ successfully substituted for $Ti^{4+}$. The results of Rietveld refinement indicated that the unit cell volume decreased when the concentration of substitution of $(Al_{1/2}Nb_{1/2})^{4+}$ increased. Raman spectra confirmed that flexible oxygen octahedra networks became stressed-rigid and oxygen octahedra became more tilted, which was ascribed to $Al^{3+}$ and $Nb^{5+}$ occupational disorder when $(Al_{1/2}Nb_{1/2})^{4+}$ crystallize into BNT ceramics. Besides, blue shift of Raman bands demonstrated that the unit cell volume decreased as $z$ increased. The relative density, packing fraction and $Q\times f$ values of BNT-(AN)$z$ ceramics 1375 °C for 4 h had a similar tendency that they all reached the maximum value at $z = 2$. For tilting octahedra structure of BNT-(AN)$z$ ceramics, the bond valence of B site increased with increase of $z$ value, and dielectric constant and $\tau_f$ value decreased accordingly, which essentially due to more tilted oxygen octahedra. Good microwave properties with $\varepsilon_r$ = 73.9, $Q\times f$ = 13,177 GHz, and $\tau_f$ = +0.3 ppm/°C were obtained for BNT-(AN)2 ceramics sintered at 1375 °C for 4 h.

## Acknowledgments

This work is supported by the Open Foundation of National Engineering Research Center of Electromagnetic Radiation Control Materials (ZYGX2016K003-5) and by National Natural Science Foundation of China (Grant No. 51402039).

## References

[1] Z. Fang, B. Tang, E. Li, S. Zhang, J. Alloys Compd. 705 (2017) 456–461.
[2] D. Zhou, W.-B. Li, H.-H. Xi, L.-X. Pang, G.-S. Pang, J. Mater. Chem. C 3 (2015) 2582–2588.
[3] Z. Fang, B. Tang, F. Si, S. Zhang, Ceram. Int. 43 (2017) 1682–1687.
[4] T. Junichi, K. Keisuke, K. Kouhei, Jpn. J. Appl. Phys. 32 (1993) 4327.
[5] R. Ubic, I.M. Reaney, W.E. Lee, Int. Mater. Rev. 43 (1998) 205–219.
[6] O. Hitoshi, O. Toshiyuki, K. Hiromichi, N. Susumu, O. Takashi, Jpn. J. Appl. Phys. 34 (1995) 187.
[7] K. Wakino, K. Minai, H. Tamura, J. Am. Ceram. Soc. 67 (1984) 278–281.
[8] H. Ohsato, J. Eur. Ceram. Soc. 21 (2001) 2703–2711.
[9] H. Chen, B. Tang, A. Gao, S. Duan, H. Yang, Y. Li, H. Li, et al., J. Mater. Sci. Mater. El 26 (2015) 405–410.
[10] Y.-P. Fu, C.-W. Liu, C.-H. Lin, C.-K. Hsieh, Ceram. Int. 31 (2005) 667–670.
[11] K.H. Yoon, W.S. Kim, E.S. Kim, Mater. Sci. Eng. B 99 (2003) 112–115.
[12] Y.J. Wu, X.M. Chen, J. Eur. Ceram. Soc. 19 (1999) 1123–1126.
[13] H. Chen, Z. Xiong, Y. Yuan, B. Tang, S. Zhang, J. Mater. Sci. Mater. El 27 (2016) 10951–10957.
[14] X. Guo, B. Tang, J. Liu, H. Chen, S. Zhang, J. Alloys Compd. 646 (2015) 512–516.
[15] E.A. Nenasheva, N.F. Kartenko, J. Eur. Ceram. Soc. 21 (2001) 2697–2701.
[16] G. Chang, X.-H. Zhou, S.-R. Zhang, T.-T. Zhang, Y.-X. Li, J. Mater. Sci. Mater. El 25 (2014) 4439–4443.
[17] X. Yao, H. Lin, X. Zhao, W. Chen, L. Luo, Ceram. Int. 38 (2012) 6723–6728.
[18] X. Huang, X. Liu, F. Liu, C. Yuan, J. Qu, J. Xu, C. Zhou, et al., J. Adv. Ceram. 6 (2017) 50–58.
[19] H. Chen, B. Tang, S. Duan, H. Yang, Y. Li, H. Li, S. Zhang, J. Electron. Mater. 44 (2015) 1081–1087.
[20] K. Momma, F. Izumi, J. Appl. Crystallogr. 44 (2011) 1272–1276.
[21] M. Rahimi, P. Kameli, M. Ranjbar, H. Hajihashemi, H. Salamati, J. Mater. Sci. 48 (2013) 2969–2976.
[22] Z. Fang, B. Tang, F. Si, S. Zhang, J. Alloys Compd. 693 (2017) 843–852.
[23] C. Gao, M. Feng, Q. Wang, Z. Yue, X. Huang, Ferroelectr 494 (2016) 76–83.
[24] R.D. Shannon, J. Appl. Phys. 73 (1993) 348–366.
[25] Y. Li, X.M. Chen, N. Qin, Y. Zeng, J. Am. Ceram. Soc. 88 (2005) 481–484.
[26] J.M. Jehng, I.E. Wachs, Chem. Mater. 3 (1991) 100–107.
[27] Q. Liao, L. Li, Dalton. Trans. 41 (2012) 6963–6969.
[28] S.K. Singh, V.R.K. Murthy, Mater. Chem. Phys. 160 (2015) 187–193.
[29] S. Wu, Y. Li, X. Chen, J. Phys. Chem. Solids 64 (2003) 2365–2368.
[30] S.Y. Wu, Y. Li, X.M. Chen, J. Appl. Phys. 96 (2004) 5683–5686.
[31] R. Muhammad, Y. Iqbal, C.R. Rambo, J. Mater. Sci. Mater. El 25 (2014) 1652–1656.
[32] H. Zheng, I. Reaney, G.C. De Györgyfalva, R. Ubic, J. Yarwood, M. Seabra, V. Ferreira, J. Mater. Res. 19 (2004) 488–495.
[33] H. Zheng, H. Bagshaw, G. Csete de Györgyfalva, I. Reaney, R. Ubic, J. Yarwood, J. Appl. Phys. 94 (2003) 2948–2956.
[34] C.-T. Chia, Y.-C. Chen, H.-F. Cheng, I.-N. Lin, J. Appl. Phys. 94 (2003) 3360–3364.
[35] I. Siny, R. Katiyar, A. Bhalla, J. Raman Spectrosc. 29 (1998) 385–390.
[36] C.W.A. Paschoal, R.L. Moreira, C. Fantini, M.A. Pimenta, K.P. Surendran, M.T. Sebastian, J. Eur. Ceram. Soc. 23 (2003) 2661–2666.
[37] W.S. Kim, E.S. Kim, K.H. Yoon, J. Am. Ceram. Soc. 82 (1999) 2111–2115.
[38] D.M. Iddles, A.J. Bell, A.J. Moulson, J. Mater. Sci. 27 (1992) 6303–6310.
[39] Y. Zhao, P. Zhang, J. Alloys Compd. 662 (2016) 455–460.
[40] Y. Zhao, P. Zhang, J. Alloys Compd. 658 (2016) 744–748.
[41] X. Yao, H. Lin, W. Chen, L. Luo, Ceram. Int. 38 (2012) 3011–3016.
[42] W. Lei, W.-Z. Lu, J.-H. Zhu, X.-H. Wang, Mater. Lett. 61 (2007) 4066–4069.
[43] E.S. Kim, B.S. Chun, D.W. Yoo, K.H. Yoon, Mater. Sci. Eng. B 99 (2003) 247–251.
[44] J.S. Kim, C.I. Cheon, T.-R. Park, H.-S. Shim, J. Mater. Sci. 35 (2000) 1487–1494.
[45] V. Matjaz, S. Danilo, J.R. Claudia, Jpn. J. Appl. Phys. 38 (1999) 2820.
[46] Y.M. Zhang, R. Ubic, D.F. Xue, S. Yang, Mater. Focus 1 (2012) 57–64.
[47] N. Brese, M. O'keeffe, Acta Crystallogr. Sect. B Struct. Sci. 47 (1991) 192–197.
[48] E.S. Kim, K.H. Yoon, J. Eur. Ceram. Soc. 23 (2003) 2397–2401.
[49] E.L. Colla, I.M. Reaney, N. Setter, J. Appl. Phys. 74 (1993) 3414–3425.